White Rose Research Online

eprints@whiterose.ac.uk
https://eprints.whiterose.ac.uk
Universities of Leeds, Sheffield and York

Deposited via The University of York.

White Rose Research Online URL for this paper:
https://eprints.whiterose.ac.uk/id/eprint/97396/

Version: Accepted Version

Proceedings Paper:
Dawson, J. F., Flintoft, I. D., Austin, A. N. et al. (2016) Shielding effectiveness of non-woven carbon fibre sheets: modelling the microstructure. In: 2016 ESA Workshop on Aerospace EMC. EUROPEAN SPACE AGENCY.

https://doi.org/10.1109/AeroEMC.2016.7504575

Reuse
Items deposited in White Rose Research Online are protected by copyright, with all rights reserved unless indicated otherwise. They may be downloaded and/or printed for private study, or other acts as permitted by national copyright laws. The publisher or other rights holders may allow further reproduction and re-use of the full text version. This is indicated by the licence information on the White Rose Research Online record for the item.

Takedown
If you consider content in White Rose Research Online to be in breach of UK law, please notify us by emailing eprints@whiterose.ac.uk including the URL of the record and the reason for the withdrawal request.

(C) 2016 European Space Agency
Dawson, J. F.; Flintoft, I. D.; Austin, A. N. & Marvin, A. C. , "Shielding effectiveness of non-woven carbon fibre sheets: modelling the microstructure" , 2016 ESA Workshop on Aerospace EMC , 23-25 May, 2016
DOI: 10.1109/AeroEMC.2016.7504575
This is an updated Author postprint with correction to figure numbering and Figure 10.

SHIELDING EFFECTIVENESS OF NON-WOVEN CARBON FIBRE SHEETS: MODELLING THE MICROSTRUCTURE

J. F. Dawson [(1)], I. D. Flintoft [(1)], A. N. Austin [(2)] , A. C. Marvin [(1)]

[(1)] Department of Electronics, University of York, York, YO1 5DD UK, john.dawson@york.ac.uk
[(2)] TFP - Global, Burneside Mills, Kendal, Cumbria , LA9 6PZ,UK, Email: andrew.austin@tfpglobal.com

ABSTRACT

This paper describes work undertaken to understand how the structure of a nonwoven carbon fibre material determines its shielding effectiveness, including the effects of fibre orientation, and contact resistance. In order to facilitate understanding of the material behaviour, software has been written to generate Monte Carlo Models (MCMs) of the material structure. The results of our MCMs are compared with measurements and some empirical expressions.

1. INTRODUCTION

There exists a large body of work on the behaviour of stick networks based on the initial work of Balberg and Binenbaum [1] mostly associated with nano-structures [2–4]. We have applied these ideas to understand the behaviour of the conductivity and shielding effectiveness of non-woven carbon fibre sheets.
Section 2 describes the structure of the nonwoven carbon fibre sheets, Section 3 summarises the shielding behaviour of the sheets and its relationship to sheet conductivity. In Section 4 we describe the MCM, and in Sections 5 and 6 we illustrate the behaviour of the conductivity of 2D and 3D materials and how anisotropy in the fibre angle distribution affects the performance. In section 7 we compare the MCM with measurements of the conductivity of real materials.

2. NON-WOVEN FABRICS

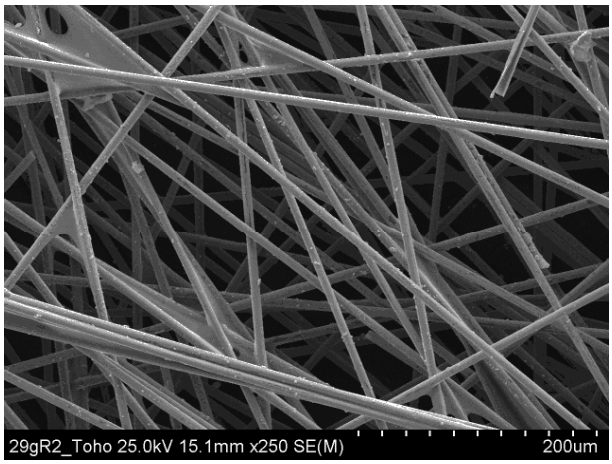

Figure 1. Electron microscope image of carbon fibre veil.

A non-woven fabric is an array of discontinuous fibres that are formed into a sheet using a wet-laid process like that used for paper manufacture. Non-woven materials possess a complicated structure with varying local parameters such as thickness, areal density, and fibre angle. Fig. 1 shows a scanning electron microscope (SEM) image of a non-woven fabric, constructed from 12 mm long carbon fibres. Non-woven carbon fibre sheets are typically incorporated in composite materials to provide a degree of conductivity where the strength and weight of a woven carbon fibre composite is not required. Sheets can be fabricated with areal densities as low as 4 gm^{-2}.

3. SHIELDING EFFECTIVNESS

Schelkunoff [5] determined the plane-wave shielding effectiveness, SE, of an infinite planar sheet in free space as:

$$SE = \frac{E_I}{E_T} = \frac{1-\left(\rho e^{-\gamma t}\right)^2}{\left(1-\rho^2\right)e^{-\gamma t}} \qquad (1)$$

where E_I is the amplitude of the normally incident plane wave, and E_T is the amplitude of the transmitted wave. γ is the propagation constant in the sheet and ρ is the interface reflection coefficient

$$\rho = \frac{\eta_m - \eta_0}{\eta_m + \eta_0} \qquad (2)$$

η_m and η_0 are the characteristic impedances of the material and of free space.
At frequencies where the skin-depth in the material is negligible the sheet conductance is the principle factor determining the electromagnetic shielding effectiveness (SE) and for high conductance materials

$$SE \approx \tfrac{1}{2}\eta_0 G_s \qquad (4)$$

where G_s is the sheet conductance. For the non-woven materials we have tested (4) is effective at frequencies up to about 2 GHz for the heaviest materials, and to beyond 8 GHz for the lightest as can be seen in Fig. 2 and in [6,7]. So in this paper we consider how the structure affects the sheet conductance and hence the SE as predicted by (4). At higher frequencies the shielding effectiveness rises due to the attenuation through the thickness of the material according to (1). That regime

is not considered in this paper.

Fig. 2 shows the measured shielding effectiveness of the heaviest and lightest samples we have measured. The areal densities shown represent the weight of carbon fibre per square metre in the material, a binder is also used which increases the actual weight by about 20%. As the materials are anisotropic, two orientations were measured using the technique described in [8]. In these materials there is considerable difference in the SE of the two difference orientations. The sheet conductance shown later was deduced by fitting the full expression (1) to the measured SE curves up to 2.5 GHz. We chose this limit as the measured SE starts to exhibit jig artefacts above this range. Fig. 2 shows the fitted data over the full frequency range (points) as well as the measured SE data (lines). It can be seen that the x-polarised values have considerable higher SE than the y-polarised cases. The values of conductances from the fit are plotted in Fig. 12.

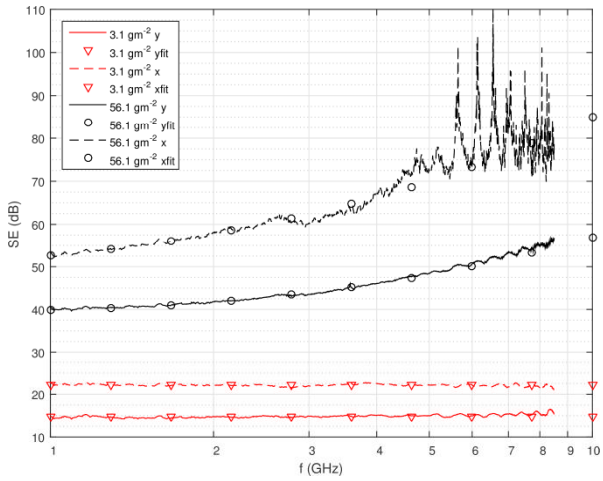

Figure 2. Shielding effectiveness of the lightest and heaviest veils at two polarisations

4. MONTE CARLO MODELS

In order to understand how the material structure affects its sheet conductance, and hence SE, we used a Monte Carlo method to construct artificial models of the structure [7].

Fig. 3 shows a rendered image of a computer generated veil model. The mass per unit area (areal density), fibre dimensions, and fibre angular distribution can be set to produce a range of material models representative of real materials. In this paper we use the model to generate a resistor network from each segment of fibre and can also include a contact resistance between fibres. Fibres with centres closer than the fibre diameter are assumed to connect and a circuit model can then be fabricated and solved using nodal analysis to determine the sheet conductance.

In order to get reliable results the model size must be at least several fibre lengths in each dimension and the results from multiple models are averaged as individual samples vary in conductance due to the stochastic nature of the material structure. In particular, at low areal density when the structure is close to the percolation threshold, large variations in conductivity can be seen from one sample to the next. The percolation threshold is the areal density where a 50% probability of connectivity across the material exists. The percolation threshold in the materials considered here is of the order of 0.03 gm^{-2}, whereas the lowest areal density available to us is 3 gm^{-2}.

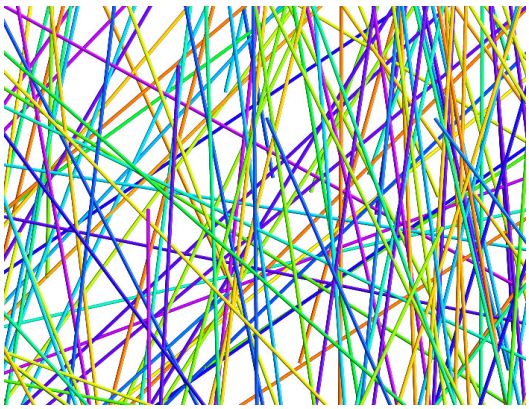

Figure 3. Computer generated veil model

5. BEHAVIOUR OF 2D MCM

Fig. 4 shows the sheet conductivity against areal density for an isotropic fibre mesh, with no contact resistance between fibres, solved in two orthogonal directions (marked x-pol and y-pol). For areal density above about 0.2 g m^{-2} it can be seen that the conductivity is proportional to areal density and the results in the two orthogonal directions are very close. At low areal density the conductivity falls more rapidly with reduction in areal density as the material approaches the percolation threshold below which point no continuous path through the fibre is likely. Žeželj and Stanković [9] modelled similar "stick-networks" and empirically determined an expression for the conductivity for the isotropic case, based on the material percolation threshold.

$$G_s = a\frac{(n-n_c)^t + c(L/l_f)}{\frac{bn^{t-1}}{G_f} + \frac{(n+n_c)^{t-2}}{G_c}} \qquad (5)$$

where G_f and G_c are the fibre and contact conductances. l_f is the fibre length, and n is the dimensionless fibre concentration: the number of fibres in an area l_f^2. n_c is the concentration of fibres at the percolation threshold, 5.63726 for isotropic 2D material. L is the size of the sample square, and $t = 1.29$ is the 2D critical exponent. The empirical constants are: $a = 0.027$, $b = 0.061$, and $c = 2.5$ as determined in [9].

The empirical fit of Žeželj and Stanković is also shown in Figs. 4-6,8,10, & 11 where the actual (marked x- and y-pol) percolation thresholds from our models are used and also for the universal threshold (marked Zezelj theory) [9].

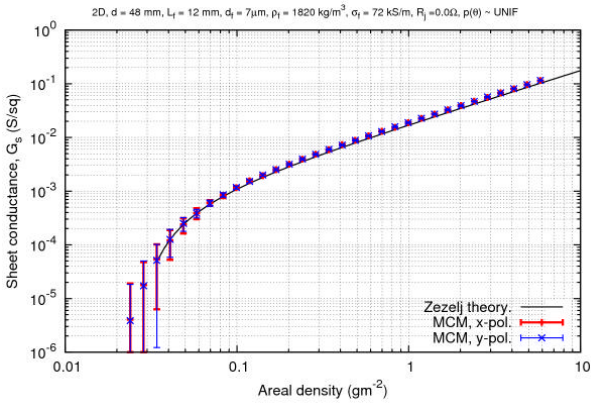

Figure 4. Sheet conductivity v areal density for uniform fibre distribution with no contact resistance, error bars show std.deviation becoming larger density reduces

Fig. 5 shows the material behaviour when the contact resistance between fibres dominates - the conductance then varies with the square of the material areal density. The reason for this is that the number of contacts per fibre increases linearly with the number of fibres present, so that the total number of contacts able to share the current increases with the square of the number of fibres.

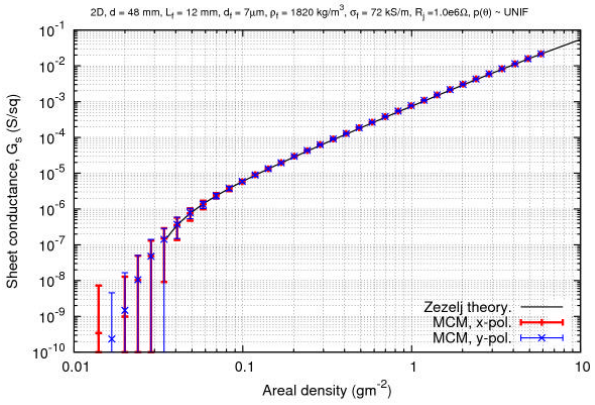

Figure 5. Effect of 1 MΩ contact resistance on veil with uniform fibre distribution.

For isotropic materials the empirical model of Žeželj and Stanković gives a good approximation of the behaviour of our models, though it does not match as well as shown in [9]. Fig. 6 shows the effect of a non-uniform distribution of fibre angles. Anisotropy can be seen in the sheet conductance when a non-uniform distribution of fibre angles is present; this is the case in most real materials.

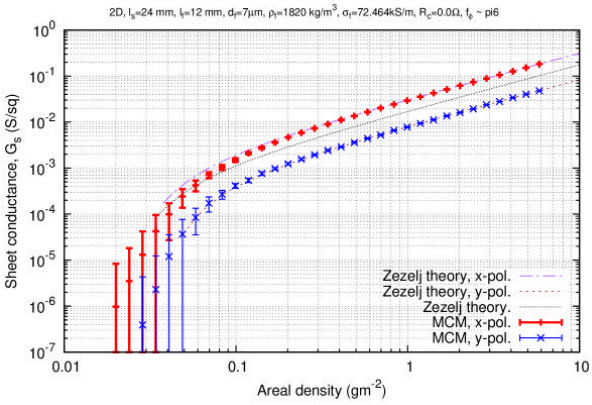

Figure 6. Sheet conductivity v areal density for truncated Gaussian fibre angular distribution $-90 \le \varphi \le 90$ deg., *with* $\sigma = 30$ deg.

It can be seen that the theory of Žeželj and Stanković does not represent the behaviour of the anisotropic case as both the level of sheet conductance, and the percolation thresholds are changed by the anisotropy. In Figure 6 we have also plotted the theory of Žeželj and Stanković modified by including the actual percolation thresholds for the x- and y-oriented directions from the Monte Carlo model, and multiplying the conductance by the factor $\Phi b/a$ where the geometry factor

$$\Phi_x = \int_{-\pi/2}^{\pi/2} \cos^2\varphi \; p(\varphi) d\varphi \qquad (6)$$

and

$$\Phi_y = \int_{-\pi/2}^{\pi/2} \sin^2\varphi \; p(\varphi) d\varphi \qquad (7)$$

where $p(\varphi)$ is the angular PDF for the fibres in the material which we have described in detail in [10] and φ is the angle of the fibre in the xy-plane, relative to the x-axis.

We also considered the average the number of contacts per fibre, which is predicted by Heitz et al [11] for the 2D isotropic case.

$$N_{cf} = n\pi P_{cont} \qquad (8)$$

where $P_{cont} = 0.2027$. This agrees well with our isotropic MCM.

Fig. 8 shows the mean number of contacts per fibre predicted by Heitz et al and the number counted in our MCM for the anisotropic material which shows a reduction.

6. BEHAVIOUR OF 3D MCM

We have observed that the main effect of the transition from 2D to 3D materials is that the number of contacts per fibre in 3D materials behaves differently from the 2D Case.

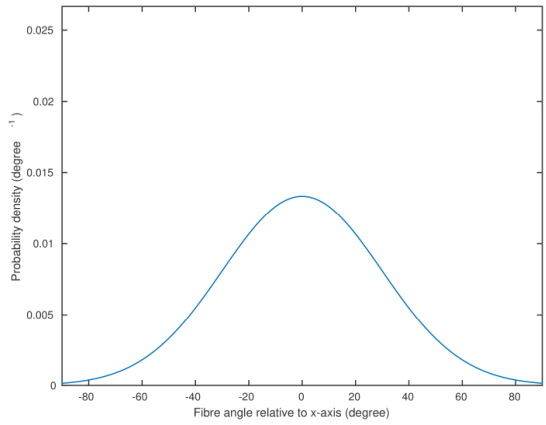

Figure 7. Truncated Gaussian fibre angle PDF $-90 \le \varphi \le 90$ deg., *with* $\sigma = 30$ deg.

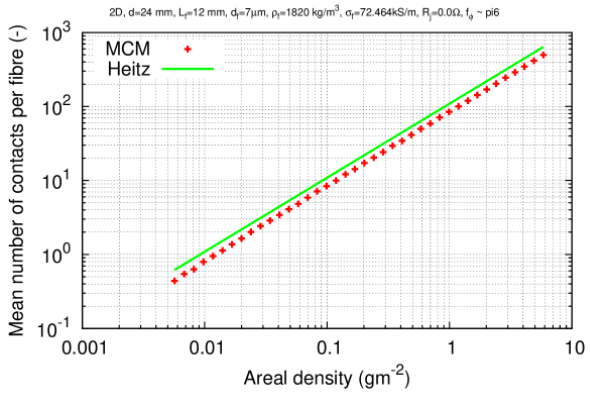

Figure 8. Number of contacts per fibre for 2D isotropic (Heitz) and anisotropic (MCM) materials.

In the plots below the thickness of the material is:

$$t = t_{\min}\sqrt{1+\left(\frac{\rho_A}{\rho_{A0}}\right)} \qquad (8)$$

where t is the material thickness between the centrelines of the outermost fibres (measured thickness minus one fibre diameter), $t_{\min} = 11.6\ \mu$m is the minimum thickness (~ 2 fibre diameters), ρ_A is the areal density and $\rho_{A0} = 1.05$ gm^{-2} is the areal density at which the material transitions from constant thickness to a linear increase in thickness with areal density. The parameters given were based on the best fit to measured thickness data [10].

The behaviour of 3D materials with zero contact resistance is identical to that of 2D materials as long as the fibres are well connected. As can be seen in Fig. 9 the number of contacts per fibre in the MCM is reduced from that of the 2D case (Heitz).

When contact resistance is significant (Fig. 10) the conductivity at larger areal densities falls below that predicted by the 2D model of Heitz as less contacts are present. Also the percolation threshold, occurs at a higher areal density as can be seen by the lowered conductance at lower densities.

In Fig. 11 a 3D veil, with a truncated Gaussian angular fibre distribution and zero contact resistance is shown. Compared with Fig. 6 the conductance is comparable at high densities but at low densities the conductance is lower due to the reduced connectivity of the fibres and again the percolation threshold occurs at a higher value than in the 2D case. This behaviour depends on how the thickness varies with areal density.

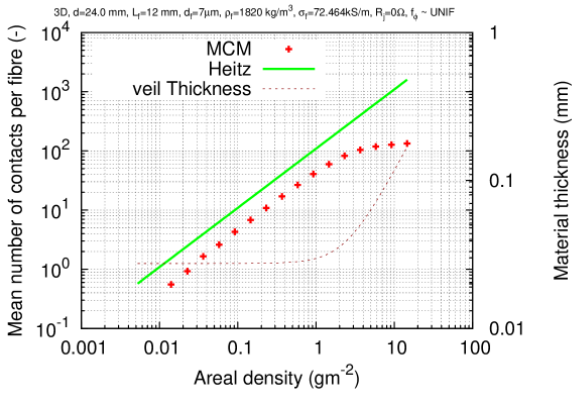

Figure 9. Material thickness and number of contacts per fibre for 3D isotropic (MCM) material compared with the 2D case (Heitz).

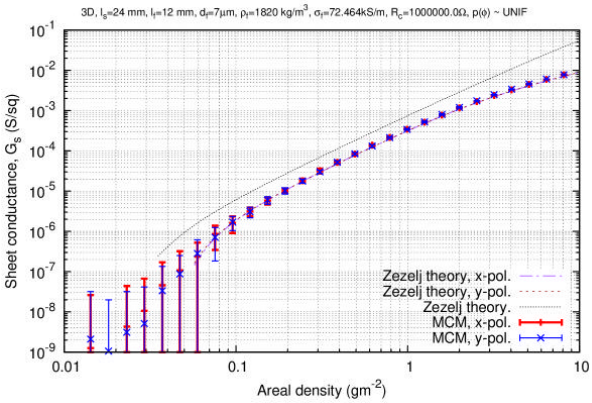

Figure 10. 3D veil with 1 MΩ contact resistance and uniform fibre distribution.

7. BEHAVIOUR OF REAL SHEETS

Fig. 11 shows the conductivity, deduced from SE measurements of a set of real materials compared with the results of the MCM prediction. The distribution of fibre angles for the real material was determined using image analysis. Also plotted is the average conductance of the materials measured with an eddy current method which can be seen to correspond well with the average predicted by the SE measurement.

The fibres in the real material have a diameter of 7 µm,

a length of 12 mm, an electrical conductivity of 72.5 kS/m and a density of 1820 kgm^{-2}. The areal density shown in this paper considers only the mass of the fibre. The binder adds about 20% to the density of the real material, but is not considered here as it does not directly affect the model. We estimate the contact resistance as approximately 8.6 kΩ by choosing a value which results in a conductivity which best fits the measured data.

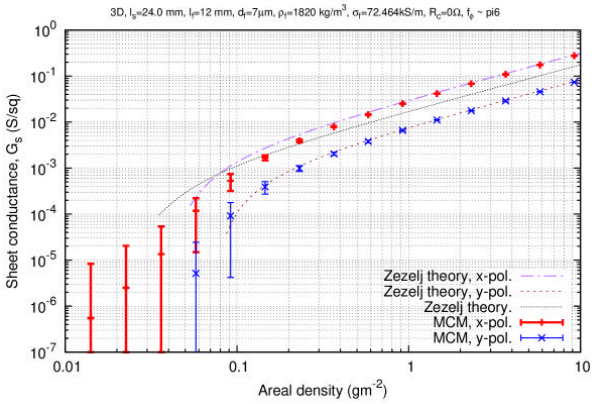

Figure 11. Sheet conductivity v areal density for truncated Gaussian fibre angular distribution $-90 \le \varphi \le 90\,\text{deg.}$, $\sigma = 30\,\text{deg.}$ *with no contact resistance.*

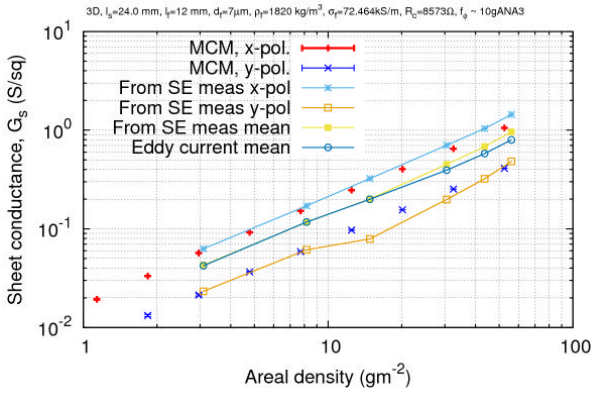

Figure 12. Comparing the sheet conductance of nowoven veils deduced from SE measurements with that of the MCM and eddy current measurements

8. CONCLUSIONS

The MCM has been a valuable tool in understanding the behaviour of nonwoven carbon fibre sheets, as previous work on stick networks concentrated on low density behaviour near the percolation threshold, and little information was available about 3D sheets. In particular the reduced number of contacts per fibre and increased percolation threshold in 3D materials suggest that contact resistance can have a significant effect on the performance of these materials.

9. REFERENCES

[1] I. Balberg and N. Binenbaum, "Computer study of the percolation threshold in a two-dimensional anisotropic system of conducting sticks," *Physical Review B*, vol. 28, Oct. 1983, p. 3799.

[2] F. Du, J.E. Fischer, and K.I. Winey, "Effect of nanotube alignment on percolation conductivity in carbon nanotube/polymer composites," *Physical Review B*, vol. 72, Sep. 2005, p. 121404(R).

[3] J. Li and M. Östling, "Conductivity scaling in supercritical percolation of nanoparticles–not a power law," *Nanoscale*, vol. 7, 2015, pp. 3424–3428.

[4] R.M. Mutiso and K.I. Winey, "Electrical percolation in quasi-two-dimensional metal nanowire networks for transparent conductors," *Physical Review E*, vol. 88, Sep. 2013, p. 032134.

[5] S.A. Schelkunoff, "The impedance concept and its application to problems of reflection, refraction, shielding, and power absorption," *Bell System Tech. J.*, vol. 17, 1938, pp. 17–48.

[6] A.N. Austin, J.F. Dawson, I.D. Flintoft, and A.C. Marvin, "Analysis of the shielding properties of metalised nonwoven materials," *Electromagnetic Compatibility (EMC EUROPE), 2013 International Symposium on*, Bruges, Belgium, 2013, pp. 526–531.

[7] A.N. Austin, J.F. Dawson, I.D. Flintoft, and A.C. Marvin, "Modelling the micro-structure of non-uniform conductive non-woven fabrics: Determination of sheet resistance," *Electromagnetic Compatibility (EMC Europe), 2015 International Symposium on*, Dresden, Germany, 2015, pp. 1–6.

[8] A.C. Marvin, L. Dawson, I.D. Flintoft, and J.F. Dawson, "A Method for the Measurement of Shielding Effectiveness of Planar Samples Requiring No Sample Edge Preparation or Contact," *IEEE Transactions on Electromagnetic Compatibility*, vol. 51, May. 2009, pp. 255–262.

[9] M. Žeželj and I. Stanković, "From percolating to dense random stick networks: Conductivity model investigation," *Physical Review B*, vol. 86, Oct. 2012.

[10] J.F. Dawson, Andrew N Austin, I.D. Flintoft, and A.C. Marvin, "Shielding Effectiveness and Sheet Conductanceof Non-woven Carbon-fibre Sheets," *Submitted to:IEEE Transactions on Electromagnetic Compatibility*, 2016.

[11] J. Heitz, Y. Leroy, L. Hebrard, and C. Lallement, "Theoretical characterization of the topology of connected carbon nanotubes in random networks," *Nanotechnology*, vol. 22, Jul. 2011, p. 345703.